XXVII Congresso Nacional de Estudantes de Engenharia Mecânica
08 a 12 de fevereiro de 2021, Curitiba, PR, Brasil

# LINEAR PLANAR DYNAMICS OF A FLUID-CONVEYING CANTILEVERED PIPE WITH A MASS ATTACHED AT THE FREE END

**Milton Aparicio de Oliveira, milton.aparicio@ufabc.edu.br**[1]
**Juan Pablo Julca Avila, juan.avila@ufabc.edu.br**[2]

[1]Federal University of ABC, milton.aparicio@ufabc.edu.br,
[2]Federal University of ABC, juan.avila@ufabc.edu.br.

***Abstract.*** *In this paper, the linear planar dynamics of a fluid-conveying cantilevered pipe with a mass attached at the free end is analyzed. Primarily, as external forces, a pulse load applied to the free end, and the self-weight of the pipe-fluid system were considered. For such loads, the dynamic behavior was analyzed for different flow velocities. Additionally, to the current external applied forces, a gravitational force has been considered, due to the end mass. The pipe was considered an Euler-Bernoulli cantilever beam having a non-negligible flexural rigidity. Only transversal, and angular displacements related to the undeformed pipe axis were considered. The fluid considered is incompressible, and the material of the pipe is elastic. The equation of motion for the model is obtained using Hamilton's variational principle. The direct integration of the dynamic equations was solved by the Newmark method. Numerical analyzes and simulations were performed using a code developed in Matlab. This paper demonstrated that in the presence of the end-mass, for different flow velocities, the system exhibits a chaotic dynamic behavior. It was demonstrated also that for increasing flow velocities the natural frequencies of the system decrease with time approaching to zero at the theoretical critical velocity.*

***Keywords****: Dynamic systems. Fluid-structure interactions.*

## 1. INTRODUCTION

Rigid pipes are of fundamental importance in riser systems for operations in the oil, and gas industry, in deep and ultra-deep water operations. The internal fluid is composed of a mixture of oil, gas, and water, flowing under different conditions of pressure, and temperature, known as slug flow. In particular, slug flow is a frequent operational phenomenon that occurs in the offshore industry. The dynamic nature of the slug pattern induces variable forces over time, leading to structural vibrations of the riser systems. These vibrations can produce considerable deflections, and stresses, which can cause excessive bending, local buckling, or failure due to fatigue. These conditions make its mathematical modeling highly complex. The study of riser systems under dynamic loads induced by a multiphase internal flow in deep waters is recent. Particularly in the offshore oil, and gas industry, there are some papers dedicated to the analysis of internal flow-conveying risers. Some authors have analyzed the dynamic behavior of the riser systems, involving relevant issues, such as the effect of the pipe flexural stiffness, the influence of large deformations, and the influence of the pulsatile internal flow, among others. Wu and Lou (1981) developed a mathematical model to study the simultaneous effect of the flow of internal fluid, and the flexural rigidity of the pipe, on the dynamic behavior of flexible risers. The authors concluded that the flexural stiffness had a great influence on the dynamic response of the riser, under internal flow at high velocities. Yamamoto (2011) carried out experiments on the effect of the flow of internal fluid, on the dynamic behavior of vertical pipes. The author noted that the pipe natural frequency tends to decrease with increasing fluid flow. Onuoha, Li, and Duan (2012) considered a linear structural model with small displacements, including the effects of axial traction. They developed the governing equation and used for its numerical resolution, the technique approximated by finite differences.

## 2. GOVERNING EQUATION

A cantilevered pipe is considered in Fig. 1. The basic hypotheses for the system are a) Flow of incompressible fluid, with constant velocity U [m/s]. b) The length of the pipe is much larger than the internal diameter. c) The vertical deflection w, and the slope $\partial w/\partial x$ is small compared with the beam's length. So that the small displacements and angle assumption shall be used. d) The flow of fluid is turbulent. e) Hook's law behavior of the pipe material is assumed. f) In

the horizontal direction, the displacements are neglected. g) The cross-sections of the deformed pipe remains orthogonal to the deformed axis.

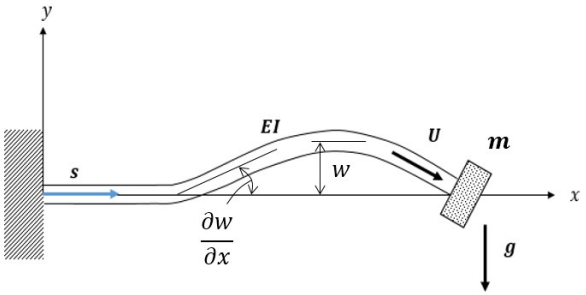


Figure 1. System scheme – Pipe with an end-mass attached at the free end.

### 2.1. Euler-Bernoulli beam model

The potential energy of a uniform beam due to bending is given by (Petyt, 2010):

$$U = \frac{1}{2}\int_0^L E\, I_z \left[\frac{\partial^2 w(x,t)}{\partial x^2}\right]^2 dx \tag{1}$$

where $E$ is the modulus of elasticity, $I_z$ the area moment of inertia of the cross-section about the neutral axis, $w(x,t)$ the transverse deflection at the axial location $x$ and time $t$, and $L$ the length of the beam. The kinetic energy of a beam is given by

$$T = \frac{1}{2}\int_0^L \rho_b\, A_b \left[\frac{\partial w(x,t)}{\partial t}\right]^2 dx \tag{2}$$

where $\rho_b$ is the density of the beam, and $A_b$ the beam cross-sectional area. If there is a distributed load, per unit length,$p_y$, then the force in the increment, $dx$, is $p_y dx$, and the work done in a virtual displacement $\delta w(x,t)$ is $\delta w(x,t)\, p_y\, dx$. The virtual work for the element is therefore

$$\delta W_{nc} = \int_0^L p_y\, \delta w(x,t) dx \tag{3}$$

The mathematical statement of Hamilton's principle is shown to be:

$$\int_{t_1}^{t_2} [\delta(T-U) + \delta W_{nc}]\, dt = 0 \tag{4}$$

Substituting equations (1), (2), and (3) in Eq. (4), and integrating by parts, gives the governing differential equation of motion for a beam:

$$EI_z \frac{\partial^4 w(x,t)}{\partial x^4} + \rho_b A_b \frac{\partial^2 w(x,t)}{\partial t^2} = p_y \tag{5}$$

The integrated terms left of Eq. (4), are given by:

$$\left[\frac{\partial^2 w}{\partial x^2}\delta\left(\frac{\partial w}{\partial x}\right)\right]_0^L = 0, \quad \left[\frac{\partial^3 w}{\partial x^3}\delta w\right]_0^L = 0 \tag{6}$$

where the first derivative $\partial w/\partial x$ is the slope, the second derivative $\partial^2 w/\partial x^2$ is the bending moment, and the third derivative $\partial^3 w/\partial x^3$ is the shear force. For equation (6) to be satisfied, the following boundary conditions hold, for the free end $(x = L)$, and for the clamped end $(x = 0)$.

$$\frac{\partial^3 w}{\partial x^3} = 0, \quad \frac{\partial^2 w}{\partial x^2} = 0, \quad \frac{\partial w}{\partial x} = 0, \qquad w = 0 \tag{7}$$

### 2.2. Fluid model

The kinetic energy for the fluid is given by:

$$T_f = \frac{1}{2}\int_0^L \rho_f A_f \left(\frac{D}{Dt}[w(x,t)]\right)^2 dx \tag{8}$$

where $\rho_f$ is the density of the fluid and $A_f$ the pipe internal cross-sectional area. The material time derivative $\frac{D}{Dt}[w(x,t)]$ for the fluid, considering the flow only in the $x$ −direction, with a constant velocity $U$ is given by (Blevins, 1994):

$$\frac{D}{Dt}[w(x,t)] = \left(\frac{\partial}{\partial t} + U\frac{\partial}{\partial x}\right) w(x,t) \tag{9}$$

where $\frac{\partial}{\partial t}$ is the partial derivative operator to $t$, and $\frac{\partial}{\partial x}$ the partial derivative operator to $x$ as the motion is planar ($z = 0$). Substituting the Eq. (9) in Eq. (8) gives the kinetic energy of the fluid:

$$T_f = \frac{1}{2}\int_0^L \rho_f A_f \left[\left(\frac{\partial}{\partial t} + U\frac{\partial}{\partial x}\right) w(x,t)\right]^2 dx \tag{10}$$

Developing the integrand of Eq. (10), and integrating by parts, the resulting equation is summed with Eq. (5), which gives the fluid-pipe system governing equation as follows:

$$E\, I_Z \frac{\partial^4 w(x,t)}{\partial x^4} + m_f\left(2\,U\frac{\partial^2 w(x,t)}{\partial t \partial x} + U^2\frac{\partial^2 w(x,t)}{\partial x^2}\right) + M_c\frac{\partial^2 w(x,t)}{\partial t^2} - p_y = 0 \tag{11}$$

where the first, and the last terms in Eq. (11) belong to the beam differential equation of motion. The second and the third terms represent, respectively, the Coriolis and the centrifugal effects on the beam's motion, due to the relative velocity of the fluid inside the pipe. The quantities defined as $m_t = \rho_b A_b$ and $m_f = \rho_f A_f$ are the linear masses of the pipe and fluid, respectively. The quantity $M_c = m_f + m_t$ is the so- called consistent mass of the system, per unit length. Then, the fourth term in Eq. (11) represents the total inertia force relative to consistent mass. It can be noted that the linear mass $m_t$ defined above, multiplied by the acceleration $\partial^2 w(x,t)/\partial t^2$ gives the pipe inertia force as in Eq. (5). That inertia force is added to the inertia force of the fluid due to the linear mass $m_f$, giving the total inertia of the system. On the other hand, it was considered only concentrated external loads applied to nodes of the system. In this paper, by hypothesis, there are no external moments applied to the system as can be seen in Fig. 1. The external concentrated loads applied at the free end of the beam are composed by the pulse load, and the weight of the end-mass attached. The pulse load $p_L = P(t)$, is a known variable force, which is a function of time. In section 4.2 of this paper, will be described what is the form of that force. The weight of the end-mass attached at the free end is $p_M = m\,g$, where $m$ is the mass of the body, and $g$ is the local gravitational acceleration. Those external concentrated loads will be applied, in advance, in section 3, in very specific positions as the components of the external nodal force vector $\{R^{ext}\}$.

## 3. SIMULATIONS BY FINITE ELEMENT ANALYSIS

### 3.1. Finite element formulation

The weak formulation is obtained by Galerkin's method applied to Eq. (12). The resulting discretization in finite elements is made by considering the nodal displacement vector $\{d(t)\}^e$ for an element $e$, dependent on time as:

$$\{d(t)\}^e = \lfloor u_1(t) \quad \theta_1(t) \quad u_2(t) \quad \theta_2(t) \rfloor^T \tag{12}$$

where, $u_1(t)$, $u_2(t)$ are nodal vertical displacements, and $\theta_1(t)$, $\theta_2(t)$ nodal rotations at nodes 1 and 2 of the typical element $e$. The externally applied loads on the element are represented by the element nodal force vector,

$$\{r_e\} = \lfloor V_1^e \quad M_1^e \quad V_2^e \quad M_2^e \rfloor^T \tag{13}$$

where $V_1^e$, $V_2^e$ are nodal shear forces, and $M_1^e$, $M_2^e$ nodal moments at nodes 1 and 2 of the element. In finite element formulation, the shape function matrix for an element, is given by:

$$[N(x)]^e = \lfloor N_1(x) \quad N_2(x) \quad N_3(x) \quad N_4(x) \rfloor \tag{14}$$

The Hermitian elements in Eq. (14) are given by (Cook, 2001):

$$N_1(x) = 1 - 3\frac{x^2}{L^2} + 2\frac{x^3}{L^3},\ N_2(x) = x - 2\frac{x^2}{L} + \frac{x^3}{L^2},\ N_3(x) = 3\frac{x^2}{L^2} - 2\frac{x^3}{L^3},\ N_4(x) = -\frac{x^2}{L} + \frac{x^3}{L^2} \tag{15}$$

where $L$ is the length of the element. The transversal displacement $w(x,t)$ of the beam is approximated in finite element analysis by the product of the shape function matrix in Eq. (14), and the nodal displacement vector in Eq. (12) as:

$$w(x,t) = [N(x)]^e\{d(t)\}^e \tag{16}$$

In this paper, the time derivatives are noted as a dot symbol over the differentiated variable, $\dot{\varphi} = d\varphi/dt$. Derivatives to $x$ are noted as $\varphi' = d\varphi/dx$. Substituting equations (12) to (16), with the corresponding derivatives in Eq. (11), gives the second-order differential equation for an element as follows:

$$[M_s]^e\{\ddot{d}(t)\} + [C]^e\{\dot{d}(t)\} + [k]^e\{d(t)\} = \{r_e\} \tag{17}$$

Using the shape functions defined in Eq. (15), and the corresponding derivatives to $x$, the matrices in Eq. (17) can be determined, by direct integration. The stiffness matrix of the element is given by, $[k]^e = E\,I\,\int_0^L [N'']^T\,[N'']dx$. Integration gives:

$$[k]^e = \frac{E\,I}{L^3}\cdot\begin{bmatrix} 12 & 6L & -12 & 6L \\ 6L & 4L^2 & -6L & 2L^2 \\ -12 & -6L & 12 & -6L \\ 6L & 2L^2 & -6L & 4L^2 \end{bmatrix} \tag{18}$$

Similarly, the system mass matrix is given by: $[M_s]^e = M_c\,\int_0^L [N]^T\,[N]dx$. After integration, gives,

$$[M_s]^e = \frac{M_c L}{420}\begin{bmatrix} 156 & 22L & 54 & -13L \\ 22L & 4L^2 & 13L & -3L^2 \\ 54 & -13L & 156 & -22L \\ -13L & -3L^2 & -22L & 4L^2 \end{bmatrix} \tag{19}$$

The Coriolis matrix is given by: $[M_D]^e = 2\,U\,m_f\,\int_0^L [N]^T\,[N']dx$, or:

$$[M_D]^e = \frac{Um_f}{30}\begin{bmatrix} 30 & -6L & -30 & 6L \\ 6L & 0 & -6L & L^2 \\ 30 & 6L & 30 & -6L \\ -6L & -L^2 & 6L & 0 \end{bmatrix} \tag{20}$$

The centrifugal force matrix is given by: $[M_C]^e = U^2\,m_f\,\int_0^L [N']^T\,[N']dx$, or:

$$[M_C]^e = \frac{U^2 m_f}{30L}\begin{bmatrix} 36 & 3L & -36 & 3L \\ 3L & 4L^2 & -3L & -L^2 \\ -36 & -3L & 36 & -3L \\ 3L & -L^2 & -3L & 4L^2 \end{bmatrix} \tag{21}$$

Starting with the mesh generation of $N$ finite elements for the structure, the linear system of second-order differential equations is assembled, as follows:

$$[M]\{\ddot{D}\} + [C]\{\dot{D}\} + [K]\{D\} = \{R^{ext}\} \tag{22}$$

In the global system, the vector $\{D\}$ is the nodal displacement vector, $\{\dot{D}\}$ is the nodal velocity vector, $\{\ddot{D}\}$ is the nodal acceleration vector, and $\{R^{ext}\}$ is the external nodal force vector. Accordingly, $[M]$ is the consistent mass matrix, $[C] = [M_D]$ is the dissipation matrix, and $[K]$ is the stiffness matrix. The global mass matrix of the fluid-pipe system, $[M_{sys}]$ is the resulting assemble of all local element-mass matrices given by Eq. (17). The local lumped end-mass matrix is given by:

$$[M_{att}]_L = m\begin{bmatrix} 0 & 0 & 0 & 0 \\ 0 & 0 & 0 & 0 \\ 0 & 0 & 1 & 0 \\ 0 & 0 & 0 & 0 \end{bmatrix} \tag{23}$$

where is $m$ the end-mass. According to the node where the end-mass is placed in the structure, the *local* end-mass matrix $[M_{att}]_L$ is assembled on the global system. The result gives the *global* end-mass matrix $[M_{att}]$, which is then summed with the consistent mass of the system $[M_{sys}]$. The matrix $[M]$ in Eq. (22), is given by (Sobrinho, 2006):

$$[M] = [M_{sys}] + [M_{att}] \tag{24}$$

### 3.2 Direct integration

In this paper, Newmark's method is used for the direct integration of the dynamic equations. The parameters for the constant average acceleration method are (Cook, 2001):

$$\alpha = \frac{1}{2}, \quad \beta = \frac{1}{4} \tag{25}$$

The Newmark's formulation is given by:

$$[K^{eff}]\{D\}_{n+1} = \{R^{ext}\}_{n+1} + [M]\left(a_0\{D\}_n + a_1\{\dot{D}\}_n + a_2\{\ddot{D}\}_n\right) + [C]\left(a_3\{D\}_n + a_4\{\dot{D}\}_n + a_5\{\ddot{D}\}_n\right) \tag{26}$$

where $[K^{eff}]$ is the effective stiffness matrix, $\{D\}_{n+1}$ is the displacement vector at $n+1$ time step, $\{R^{ext}\}_{n+1}$ is the external load vector at $n+1$ time step, $\{D\}_n$, $\{\dot{D}\}_n$, and $\{\ddot{D}\}_n$ are the displacement, velocity, and acceleration vectors at $n$ time step, respectively. The acceleration and velocity vectors, calculated at time $n+1$ are given, respectively, by:

$$\{\ddot{D}\}_{n+1} = a_0\left(\{D\}_{n+1} - \{D\}_n - \Delta t\{\dot{D}\}_n\right) - a_2\{\ddot{D}\}_n \tag{27}$$

$$\{\dot{D}\}_{n+1} = a_3(\{D\}_{n+1} - \{D\}_n) - a_4\{\dot{D}\}_n - a_5\{\ddot{D}\}_n \tag{28}$$

The effective matrix for the system is given by:

$$[K^{eff}] = a_0[M] + a_3[C] + [K] \tag{29}$$

The acceleration vector $\{\ddot{D}\}_0$ is obtained by:

$$\{\ddot{D}\}_0 = [M]^{-1}\left(\{R^{ext}\}_0 - [K]\{D\}_0 - [C]\{\dot{D}\}_0\right) \tag{30}$$

where the initial displacement vector $\{D\}_0$ is given by the static analysis of the beam. In this paper, the initial velocity $\{\dot{D}\}_0$ is assumed zero. As the mass matrix $[M]$ is a non-singular symmetric matrix, it has an inverse that can be substituted in Eq. (30) to obtain the initial acceleration vector $\{\ddot{D}\}_0$. The Newmark remaining integration parameters are given by:

$$a_0 = \frac{1}{\beta\Delta t^2}, a_1 = \frac{1}{\beta\Delta t}, a_2 = \frac{1}{2\beta} - 1, a_3 = \frac{\alpha}{\beta\Delta t}, a_4 = \frac{\alpha}{\beta} - 1, a_5 = \Delta t\left(\frac{\alpha}{2\beta} - 1\right) \tag{31}$$

where $\Delta t$ is the incremental time step. The calculations routine starts with the determination of the initial acceleration vector in Eq. (30), with the external load vector $\{R^{ext}\}_0$, the displacement vector $\{D\}_0$, and the velocity vector $\{\dot{D}\}_0$ known from the initial conditions. Then, Eq. (26) is solved for $\{D\}_1$ by the solution of a set of linear algebraic equations, as the external load, the dumping, and the stiffness matrices of the system are known to each time step. Next, with Eq. (27), and Eq. (28) can be obtained the vectors $\{\ddot{D}\}_1$, and $\{\dot{D}\}_1$. In the next step, Eq. (26) is solved for $\{D\}_2$, and so on.

## 4. RESULTS

In the finite element analysis, 40 elements were used. The total time analysis is $4,0[s]$ with equal time steps of $\Delta t = 0,01\ [s]$. The free span of the beam has a length of $1{,}0\ [m]$. The outside diameter of the pipe is $10{,}0\ [mm]$, with a wall thickness of $0,1\ [mm]$. The pipe material is steel, with $207\ [GPa]$ elastic modulus, and a density of $8.000\ [kg/m^3]$. The fluid considered is water, with a density of $1.000\ [kg/m^3]$. The fluid was considered with a constant velocity $v_f = U\ [m/s]$. It was considered a set of different flow velocities to study the dynamic behavior of the system. The data and parameters used are in agreement with those found in (Grant, 2010), to compare the results obtained.

### 4.1 Static analysis

For comparison of FEA static analysis with the theoretical results, a point load of $-6.1 \times 10^{-1}$ $[N]$ was applied due to end-mass weight attached at the free end of the pipe. Moreover, it was considered the distributed load due to the pipe and the fluid self-weights per unit length. The deformation along the horizontal axis is shown in Fig. 2a. The theoretical static deflection at the free end, due to linear pipe & fluid weights, and the applied gravitational force of the end-mass is given by (Timoshenko, 1986): $f_{th} = \frac{L^3}{24EI}\left[3 \cdot \left(m_t + m_f\right) \cdot L + 8 \cdot m \cdot g\right]$. Substitution of the problem data, gives $f_{th} = -0.0415$ $[m]$. The result for FEA, given by the Matlab code is $f_{FEA} = -0.0415$ $[m]$. It can be seen that the values agree, for both theoretical, and FEA static analysis.

### 4.2 Dynamic analysis

Primarily, the natural frequencies of the system for two load conditions - the pipe full of fluid, and with the addition of the end-mass over the previous condition, were analyzed. For both conditions, the flow velocity is zero. The dynamic load was applied to the system by a pulse load with the intensity of $2 \times 10^{-1}$ $[N]$, downward, during the time interval of $0,01$ $[s]$. It can be seen in Table 1 the values of oscillation- amplitudes and periods, for the two configurations, that is, with and without the end-mass attached at the free end. The vertical displacement of the free end is therefore due only to the pulse load applied. After that, for comparison of the dynamic behavior, is placed an end-mass $m = 0.0675$ $[kg]$ at the free end. The dynamic response of the system is shown in Fig. 2b. The variation for the amplitude with the end-mass, relative to the free motion, for $v_f = 0$ $[m/s]$ is $0.0321/0.0307 = 1.0456$, or, $+4.56\%$. That is, the amplitudes in both cases are approximately the same with a low percentage of variation. Thus, the dynamic rigidity of the system does not vary significantly by the presence of the end-mass, for the case of full-pipe with no flow of fluid. On the other hand, the variation of the period of oscillation is $0.3441/0.1854 = 1.8562$, or, $+85.62\%$. The effect of the end-mass on the oscillation-period of the beam is significantly greater than the configuration without the end-mass. Conversely, the frequency is reduced by $-46.12\%$, with a value of $2.906$ $[Hz]$.

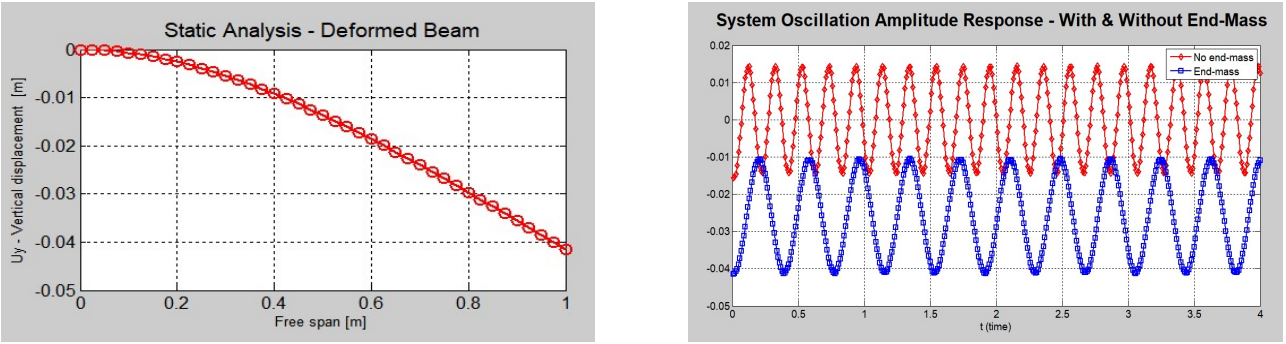


Figure 2a) Static deformation of the beam. 2b) Dynamic behavior for free vibration for full pipe-beam $\left(v_f = 0\ [m/s]\right)$.

Table 1. Amplitudes and periods of oscillations for different configurations

| **Configuration** | **Amplitude** [m] | **Period [s]** |
|---|---|---|
| No end-mass | 0.0307 | 0.1854 |
| End-mass | 0.0321 | 0.3441 |

The new dynamic equilibrium point is $-0.026$ $[m]$. It has to be noted that all values were given by Matlab code (see Fig. 3). The end-mass had dislocated the dynamic equilibrium point to a new position, due to gravity. Thus, the main effects observed due to end-mass on the dynamic behavior were to decreasing the oscillation-frequency due to inertia, and to dislocating the dynamic equilibrium to a new point due to gravity. Its influence was not to dumping the oscillation-amplitude of the system, as expected. Indeed, the observed amplitudes in both configurations were approximately the same, as can be seen in Table 1. Next, the pipe is full of water, with a fixed flow velocity $vf = 1.5$ $[m/s]$, and with variable end-masses attached. The dynamic behavior is shown in Fig. 3a. Now, the system presents a dumping character oscillation. For the end-mass equals to zero kilograms, the system oscillates about the zero vertical dynamic equilibrium point. This is shown in red color in Fig. 3a. For the end-masses of $m = 0.0625$ $[kg]$, and $m = 0.100$ $[kg]$ the system is dislocated to a new equilibrium-point, according to each mass, downward, by the gravity force, as before. Again, the masses have the effect of reducing the system-frequencies. It can be observed that for increasing mass values the system oscillates in increasing time intervals. With no mass, in about 2.0 [s] the oscillatory amplitude is near to zero. On the other hand, for a mass of $0.100$ $[kg]$, after $4.0$ $[s]$ the oscillation-amplitude is still present. This is due to the combined actions on the system response due to the dumping effect of Coriolis forces, the

lifting effect of the centrifugal forces with time, besides the increased oscillation-periods due to the inertia of the end-masses. Next, is attached the end-mass of a fixed value of $m = 0.0625\ [kg]$ at the free end. The system behavior is again dynamically dumped due to fluid flow. Same as above, the effect of the end-mass is to dislocating the equilibrium point of the system downward, to a new dynamic equilibrium point located at approximately $-0.026\ [m]$, bellow the null vertical equilibrium point, as it can be seen in Fig. 3b. The value found was the same for the simulation as shown in Fig. 2b. As it can be seen in Fig. 3b, with a fixed value of end-mass, increasing values of flow velocities induce increasing dumping effects on the system. It can be noted that for flow velocity of $30\ [m/s]$ the dumping effect is severe, with very little oscillations, after approximately $0.34\ [s]$. Furthermore, for t=0 [s] the system starts from a point bellow $-0.0415\ [m]$, valid for all anterior analysis data, that is, starts from the point $-0{,}0454\ [m]$, and stabilizes at a point at approximately $-0{,}0284\ [m]$ which is also, different from the anterior equilibrium point, i.e., $-0.026\ [m]$. This particular dynamic behavior can be explained as the result of the superposition of the combined effects of the fluid flow, and the weight of the end-mass. The fluid flow tends to lift the end-mass, due to centrifugal forces acting upward. The Coriolis acceleration of fluid flow contributes to the dumping behavior of the system.

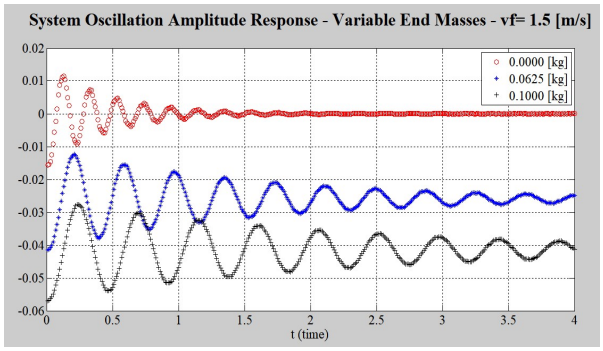


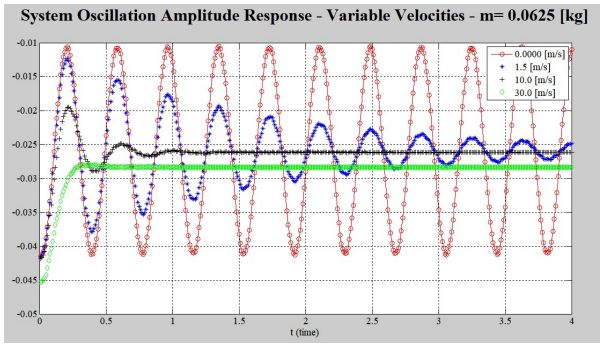


Figure 3a) Dynamic dumping behavior of the beam. 3b) Dynamic dumping behavior of the beam in the presence of end-mass $m = 0.0625\ [kg]$, combined with variable flow velocities.

On the other hand, the weight of the end-mass pushes the whole system in a downward direction due to the gravitational field. Finally, the frequency responses of the system were analyzed. The flow velocity ratio increases, the frequency ratio of the system decreases. The first critical frequency for the pipe-fluid system from Rayleigh-Ritz exact solution is given by $w_c = \frac{3.516}{L^2} \cdot \sqrt{\frac{E \cdot I}{m_f + m_p}} = 31.18\ [\frac{rd}{s}]$, where the linear masses $m_f,\ m_p$ are referred to as the fluid and pipe linear masses, respectively. In the presence of the dumping effect, the numerical value of the minimum natural frequency of the system is given by the minimum absolute value of the imaginary parts of the eigenvalues from the Hermitian matrix, $H = \begin{bmatrix} -M^{-1}C & -M^{-1}K \\ 0 & I \end{bmatrix}$.

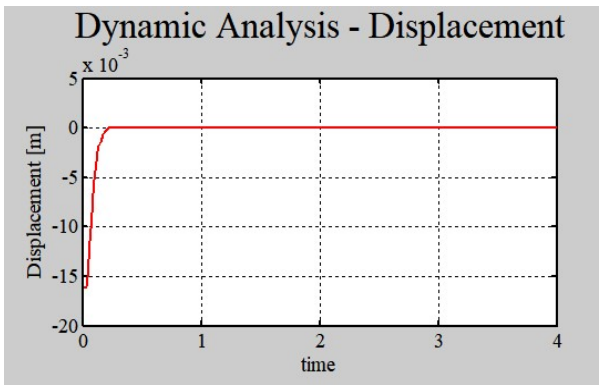


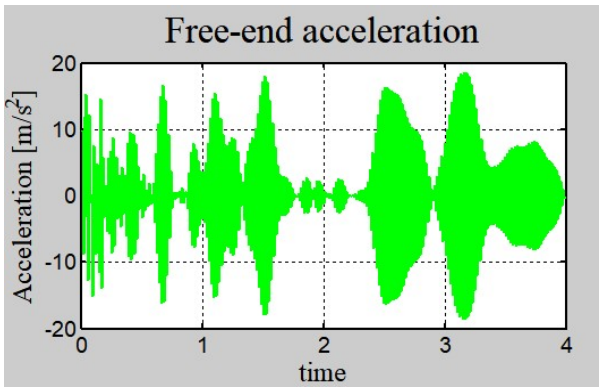


Figure 4a) Dynamical response at the critical velocity $v_c = 19.17\ [m/s]$. 4b) Chaotic form of acceleration at the free-end with the critical flow velocity $v_f = 19.17\ [m/s]$

At the critical flow velocity $v_c = \frac{1.875}{L} \cdot \sqrt{\frac{E \cdot I}{m_f}} = 19.17\ [\frac{m}{s}]$ the displacement at the free end starts from $-16\ \times\ 10^{-3}\ [m]$ and goes to zero in about $0.2\ [s]$ (see Fig. 4a). It can be seen in Fig. 4b the chaotic behavior of the acceleration at the free end of the pipe, with the critical flow velocity of $19.17\ [m/s]$.

## 5. CONCLUSION

The fluid-pipe system, in the presence of the end-mass, for different flow velocities, starts with the characteristic of a phenomenon known as jump, followed by a damped oscillation, over time. The combined effects of Coriolis and Centrifugal forces have a remarkable influence on the system dynamic behavior. The Coriolis Effect acts as a damping force reducing the system amplitude oscillation, over time. On the other hand, the Centrifugal forces tend to raise the fluid-pipe system as a whole. Additionally, the combined action of these two forces, with the gravitational force acting on the end-mass, is to move the dynamic equilibrium point to a new point located above the static equilibrium point. Another important point refers to the influence of the fluid flow velocity on the dynamic response of the system. As the flow velocities increase, the natural frequencies of the system decrease. In addition, the system has a chaotic behavior at the theoretical critical flow rate. We note here that some limitations assumed in this article significantly influence the results of the dynamic behavior of the system. This opens the need to take into account, in future analyzes, some hypotheses such as variable flow density, horizontal displacements, and shear effects, citing only some of them.

## 6. ACKNOWLEDGEMENTS

I would like to thank all the people that had influenced and contributed to the realization of this paper. In particular, I wish to thank ABCM for the publishing of this paper. I would like to thank also, my tutor, Ph.D. Juan Pablo Julca Avila for your great help, and brilliant opinions on the present work. Moreover, I dedicate this work for my wife Rose, and my sons Rafael, and Michelle.

## 7. REFERENCES

Blevins, Robert D., “Flow-Induced Vibration.” 2nd ed., Krieger, 1994.
Cook, Robert Davis, “Concepts and applications of finite element analysis.” 4th ed, Wiley, 2001.
Grant, I., “Flow-induced vibrations in pipes, a finite element approach.” Thesis, Cleveland State University, 2010.
Onuoha, Mac D.U., Li, Q., Duan, M., “On the interaction between severe slug buildup and dynamic response of a submerged top-tensioned riser.”, Conference: ASME, 31st International Conference on Ocean, Offshore and Arctic Engineering, 2012.
Petyt, M., “Introduction to finite element vibration analysis”, 2nd ed., Cambridge University Press, 2010.
Sobrinho, A. S. C., “Introdução ao método dos elementos finitos”, 1st ed., Editora Ciência Moderna, 2006.
Timoshenko, Stephen. “Strength of Materials”, CBS Publishers & Distributors, 1986.
Wu, M., Lou, J., “Effects of rigidity and internal flow on marine riser dynamics”, Applied Ocean Research, Volume 13, Issue 5, Pages 235-244, October 1991.
Yamamoto, M., “A study about the dynamic behavior of flexible pipes including internal flow”, Thesis, Yokohama National University, 2011.

## 8. RESPONSIBILITY NOTICE

The authors are the only responsible for the printed material included in this paper.